Quasiparticle and Nonquasiparticle Transport in Doped Quantum Paraelectrics

Abhishek Kumar[,1] Vladimir I. Yudson,[2,3] and Dmitrii L. Maslov[1]

[1]*University of Florida, Gainesville, Florida 32611, USA*
[2]*Laboratory for Condensed Matter Physics, National Research University "Higher School of Economics"*
20 Myasnitskaya Street, Moscow 101000, Russia
[3]*Russian Quantum Center, Skolkovo, Moscow 143025, Russia*

Charge transport in doped quantum paraelectrics (QPs) presents a number of puzzles, including a pronounced T^2 regime in the resistivity. We analyze charge transport in a QP within a model of electrons coupled to a soft transverse optical (TO) mode via a two-phonon mechanism. For T above the soft-mode frequency but below some characteristic scale (E_0), the resistivity scales with the occupation number of phonons squared, i.e., as T^2. The T^2 scattering rate does not depend on the carrier number density and is not affected by a crossover between degenerate and nondegenerate regimes, in agreement with the experiment. Temperatures higher than E_0 correspond to a nonquasiparticle regime, which we analyze by mapping the Dyson equation onto a problem of supersymmetric quantum mechanics. The combination of scattering by two TO phonons and by a longitudinal optical mode explains the data quite well.

Quantum paraelectrics (QPs) are materials close to a ferroelectric transition but never quite making it because of zero-point motion which disrupts symmetry breaking [1–4]. This group includes several perovskites, e.g., SrTiO$_3$ (STO), KTaO$_3$ (KTO), and EuTiO$_3$ (ETO), and a number of rock salts, e.g., PbTe. Electron transport in doped QPs is very much different from that in doped semiconductors. To begin with, a very large static dielectric constant ($\sim 25\,000$ in STO) translates into a micron-long Bohr radius. Consequently, conduction in QPs sets in at very low doping, e.g., at few times 10^{15} cm^{-3} carriers in STO [5], and is prominently metallic above 10^{17} cm^{-3}. In the metallic regime, the resistivity increases by several orders of magnitude from the liquid helium to room temperatures, exceeding the Mott-Ioffe-Regel (MIR) limit around 100 K [6]. A very intriguing observation is a prominent T^2 scaling of the resistivity observed in STO [7–9], KTO [10], and ETO [11]. Normally, a T^2 resistivity is associated with the Fermi-liquid (FL) behavior. However, a T^2 resistivity in QPs is observed already at very low doping, when umklapp scattering is forbidden and only the lowest conduction band is occupied [7], and straddles a number of relevant energy scales, such as the plasma frequency and the Fermi energy (E_F). In addition, the T^2 scattering rate depends only weakly on the electron number density n [7,8]. All of the above contradicts the interpretation of the T^2 behavior in terms of the FL theory [3,8,12,13].

In this Letter, we discuss the model of electrons interacting with a soft transverse optical (TO) mode, which is a defining feature of QPs. As temperature is lowered, the frequency of the TO mode decreases, indicating the tendency to a ferroelectric transition, but eventually saturates at a small but finite value (as low as $\omega_0 \approx 1$ meV for the E_u mode in STO [14–16]). For electrons near the Brillouin zone center, single-TO phonon scattering is suppressed in a single-band system and in the absence of spin-orbit interaction [17–22], and the lowest-order process involves two TO (2TO) phonons [23–25].

We show that the model is characterized by a material-dependent energy scale E_0, separating the regimes of quasiparticle and nonquasiparticle transport, at lower and higher T, respectively. (In STO, E_0 is on the order of 100 K.) For $\omega_0 \ll T \ll E_0$, the TO mode is in the classical regime, and a T^2 term in the resistivity arises simply from the square of the phonon occupation number. A unique feature of the 2TO mechanism is that the quasiparticle scattering rate, $1/\tau \sim T^2/E_0$, does not depend on the electron energy. This explains why the observed T^2 scattering rate depends on n only weakly for $T \ll E_F$ and does not exhibit a crossover at $T \sim E_F$.

For $T \gg E_0$, the quasiparticles are not well defined. By mapping the Dyson equation for the self-energy onto an exactly soluble problem of supersymmetric quantum mechanics, we show that transport in this regime is dominated by severely *off-shell* electrons. In this regime, the resistivity scales as $T^{3/2}$ and violates the MIR limit.

Finally, we show that a more realistic model, which incorporates the T dependence of the TO soft mode and also includes scattering by longitudinal optical (LO) phonons, explains the experimental data, *if the freeze-out of TO phonons for $T < \omega_0$ is ignored.* We discuss the advantages and shortcomings of the 2TO model and propose a number of experiments that can falsify it.

We consider 3D electrons coupled to an O(3) electric polarization $\mathbf{P}(\mathbf{r})$, produced by TO phonons. Because $\boldsymbol{\nabla} \cdot \mathbf{P} = 0$, single-phonon coupling is forbidden and the Hamiltonian starts with a two-phonon term [24–26]

$$H_{2\mathrm{TO}} = \frac{g_2}{2} \int d^3 r \mathbf{P}^2(\mathbf{r}) \psi^{\dagger}(\mathbf{r}) \psi(\mathbf{r}), \qquad (1)$$

where g_2 is the coupling constant (with units of the volume). Other than allowing for TO modes, we treat the material as isotropic. For a TO mode with dispersion $\omega_{\mathbf{q}}^2 = \omega_0^2 + s^2 q^2$ and polarization $\mathbf{e}_{\mathbf{q}}^a$,

$$\mathbf{P}(\mathbf{r}) = \sum_{\mathbf{q},a} \frac{\mathbf{e}_{\mathbf{q}}^a}{\sqrt{V}} A_{\mathbf{q}} b_{\mathbf{q}} e^{i\mathbf{q}\cdot\mathbf{r}} + \mathrm{H.c.}, \qquad (2)$$

where $A_{\mathbf{q}}^2 = [\varepsilon_0(\mathbf{q}) - \varepsilon_\infty]\omega_{\mathbf{q}}/4\pi$ [34]. The sum over $a = 1, 2$ accounts for two (degenerate) branches of the TO mode, $\varepsilon_0(\mathbf{q})$ and ε_∞ are the static and high-frequency limits of the dielectric function, respectively, and $b_{\mathbf{q}}$ is the bosonic annihilation operator. The diagrams for the electron self-energy are shown in Fig. 1, where the solid and wavy lines denote the (Matsubara) electron and phonon Green's functions, $G(\mathbf{k}, \epsilon_m)$ and $D(\mathbf{q}, \omega_m)$, respectively, and solid dots denote the electron-2TO-phonon vertex $\Gamma_{\alpha\beta}(\mathbf{q}) = g_2 A_{\mathbf{q}}^2 (\delta_{\alpha\beta} - q_\alpha q_\beta/q^2)$. Phonons will be treated as bare ones; hence $D(\mathbf{q}, \omega_m) = -2\omega_{\mathbf{q}}/(\omega_m^2 + \omega_{\mathbf{q}}^2)$.

We now focus on the classical regime, when phonons can be treated as static "thermal disorder" [35], which corresponds to setting $\omega_m = 0$ in the phonon lines. After analytic continuation $i\epsilon_m \to \epsilon + i0^+$, Fig. 1(a) yields
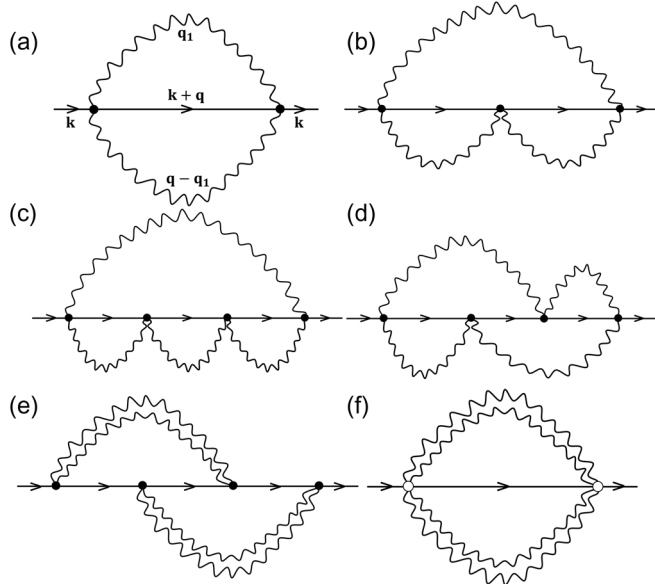

(a) (b) (c) (d) (e) (f)

FIG. 1. Diagrams for the electron self-energy due to scattering by TO phonons. (a) Two-loop two-phonon diagram. (b),(c) Three- and four-loop "umbrella" diagrams without crossings. (d),(e) Examples of diagrams with crossings. (f) Four-phonon diagram resulting from adding a $\mathbf{P}^4$ term to Eq. (1).

$$\Sigma(\mathbf{k}, \epsilon) = \int_{\mathbf{q}} G(\mathbf{k} + \mathbf{q}, \epsilon) U(\mathbf{q}), \qquad (3)$$

where the correlation function of thermal disorder is

$$U(\mathbf{q}) = 2T^2 \int \frac{d^3 q_1}{(2\pi)^3} \sum_{\alpha\beta} \frac{\Gamma_{\alpha\beta}(\mathbf{q}_1)}{\omega_{\mathbf{q}_1}} \frac{\Gamma_{\beta\alpha}(\mathbf{q} - \mathbf{q}_1)}{\omega_{\mathbf{q}-\mathbf{q}_1}}. \qquad (4)$$

Other diagrams can be treated in a similar manner.

We also assume for now that the material is very close to the quantum-critical point, so that the gap in the phonon dispersion can be neglected, i.e., $\omega_{\mathbf{q}} = sq$. Neglecting also ε_∞ compared to $\varepsilon_0(\mathbf{q})$ and excluding $\varepsilon_0(\mathbf{q})$ via the Lyddan-Sachs-Teller (LST) relation $\varepsilon_0(\mathbf{q}) = \Omega_0^2/\omega_{\mathbf{q}}^2$ and integrating over $\mathbf{q}_1$, we obtain

$$U(\mathbf{q}) = \frac{3\pi}{2m^* q} \frac{T^2}{E_0} \quad \text{with} \quad E_0 \equiv \frac{64\pi^3 s^4}{m^* g_2^2 \Omega_0^4}, \qquad (5)$$

where E_0 is characteristic energy scale of the model. The $1/q$ scaling of $U(\mathbf{q})$ (or $1/r^2$ scaling is real space) will be crucial in what follows.

For $T \ll E_0$, thermal disorder is weak. This is the quasiparticle regime, when Fig. 1(a) with G replaced by its free-electron form, $G_0(\mathbf{k}, \epsilon) = (\epsilon - \xi_{\mathbf{k}} + \mu + i0)^{-1}$ with $\xi_{\mathbf{k}} = k^2/2m^*$, gives the leading-order result. Accounting also for a transport correction, we obtain the standard result for the transport scattering rate

$$\frac{1}{\tau} = 2\pi \int \frac{d^3 q}{(2\pi)^3} \delta(\xi_{\mathbf{k}+\mathbf{q}} - \xi_{\mathbf{k}}) U(\mathbf{q})(1 - \cos\theta), \qquad (6)$$

where θ is the angle between $\mathbf{k}$ and $\mathbf{k} + \mathbf{q}$. (The difference between the quantum and transport rates is insignificant because our thermal disorder is relatively short ranged; as a result, the two rates differ only by a factor of $2/3$.)

In general, τ depends on the electron energy $\xi_{\mathbf{k}}$ via the electron density of states. This is the reason why, for example, the resistivity of a semiconductor due to acoustic phonon scattering scales as T for $T \ll E_F$ and as $T^{3/2}$ for $T \gg E_F$. Our case of $U(\mathbf{q}) \propto 1/q$ is, however, special: the $1/q$ factor cancels out with the density of states, and the result does not depend on $\xi_{\mathbf{k}}$. Evaluating also Figs. 1(b) and 1(c), we obtain

$$\frac{1}{\tau} = \frac{T^2}{E_0} - 1.24 \frac{T^3 \sqrt{m^*}}{k E_0^{3/2}} + \mathcal{O}\left(\frac{T^5 m^{*3/2}}{k^3 E_0^{5/2}}\right). \qquad (7)$$

The leading term in Eq. (7) is the most relevant one for the experiment: because it does not depend on $\xi_{\mathbf{k}}$, its thermal average does not depend on the statistics of charge carriers, and the corresponding resistivity

$$\rho = \frac{m^*}{ne^2}\frac{T^2}{E_0} \tag{8}$$

scales as T^2 regardless of whether T is lower or higher than E_F. From the data [36], we extract $E_0 = 209$ K in STO at $n = 4 \times 10^{17}$ cm^{-3}. Using the known parameters of the phonon spectrum [37] ($s = 6.6 \times 10^5$ cm/s and $\Omega_0 = 194.4$ meV) and $m^* = 1.8m_0$ [38], we find that $E_0 = 209$ K corresponds to $g_2 = 0.60a_0^3$, where $a_0 = 3.9$ Å is the STO lattice constant. This is close to an earlier estimate [24,25] of $g_2 = 1.0a_0^3$.

Strong thermal disorder ($T \gg E_0$) corresponds to a nonquasiparticle regime. Since $E_F \ll E_0$ for the relevant range of electron number densities, we will consider the nondegenerate case only. According to Eq. (7), $1/\tau$ becomes comparable to the electron energy (T) at $T \sim E_0$. If TO scattering is treated as purely elastic, the condition $T\tau \sim 1$ should indicate the onset of Anderson localization. However, small but finite energy transfers give rise to dephasing, which turns out to be strong enough to prevent localization. Indeed, in a typical scattering event, electron energy is changed by $\delta\epsilon \sim k_T s$, where $k_T \sim \sqrt{m^*T}$ is the thermal electron momentum. This corresponds to diffusion along the energy axis with a diffusion coefficient $\mathcal{D}_\epsilon \sim (\delta\epsilon)^2/\tau \sim m^* s^2 T^3/E_0$. The phase-breaking time τ_ϕ can be estimated from the condition that the phase accumulated during τ_ϕ is on the order unity [39], i.e., $\Delta\phi = \Delta\epsilon\tau_\phi = (\mathcal{D}_\epsilon\tau_\phi)^{1/2}\tau_\phi \sim 1$ or $\tau_\phi \sim (E_0/m^*s^2)^{1/3}/T$. We see that τ_ϕ becomes comparable to the elastic time $\tau \sim E_0/T^2$ at $T \sim T_\phi = (m^*s^2/E_0)^{1/3}E_0 \ll E_0$, i.e., already in the quasiparticle regime, and it is reasonable to assume that localization can be neglected for all $T > T_\phi$.

We now find the self-energy self-consistently from Dyson equation (3). Relabeling $\mathbf{q} = \mathbf{k} - \mathbf{k}'$ and integrating over the angle between $\mathbf{k}$ and $\mathbf{k}'$, we obtain

$$\Sigma(\xi, \epsilon) = \lambda \int_0^\infty d\xi' K(\xi, \xi') \frac{1}{\tilde{\epsilon} - \xi - \Sigma(\xi', \epsilon)}, \tag{9}$$

where $\tilde{\epsilon} = \epsilon + \mu$, $\lambda = 3T^2/4\pi E_0$, $\xi \equiv \xi_{\mathbf{k}}$, $\xi' \equiv \xi_{\mathbf{k}'}$, and $K(\xi, \xi') = \sqrt{\xi'/\xi}\Theta(\xi - \xi') + \Theta(\xi' - \xi)$. At weak coupling ($T \ll E_0$), when Green's function can be replaced by its free-electron form, $\mathrm{Im}\Sigma(\xi, \epsilon) = -\pi\lambda\Theta(\tilde{\epsilon})[\Theta(\xi - \tilde{\epsilon})\sqrt{\tilde{\epsilon}/\xi} + \Theta(\tilde{\epsilon} - \xi)]$ is nonzero only above the bottom of the band [40]. We will now show that at strong coupling ($T \gg E_0$) the threshold in $\mathrm{Im}\Sigma(\xi, \epsilon)$ moves from $\tilde{\epsilon} = 0$ to a finite value that depends on the coupling constant. This is an essentially nonperturbative effect that defines transport in the nonquasiparticle regime.

If a threshold does exist, $\mathrm{Im}\Sigma(\xi, \epsilon)$ must be small right above the threshold. Therefore, Eq. (9) can be expanded in $\gamma_\epsilon(\xi) \equiv -\mathrm{Im}\Sigma(\xi, \epsilon)$. On the other hand, $\mathrm{Re}\Sigma(\xi, \epsilon)$ is expected to be regular near the threshold and to depend on ξ only weakly, so it can be absorbed into the chemical

potential. (Using Kramers-Kronig relation, one can show that $\mathrm{Re}\Sigma$ depends on ξ and ϵ only logarithmically [26].) Assuming that relevant $\tilde{\epsilon} < 0$, we expand the imaginary part of Eq. (9) in $\gamma_\epsilon(\xi)$ as

$$\gamma_\epsilon(\xi) = \lambda \int_0^\infty d\xi' K(\xi'/\xi)\left(\frac{\gamma_\epsilon(\xi')}{(\tilde{\epsilon} - \xi')^2} - \frac{\gamma_\epsilon^3(\xi')}{(\tilde{\epsilon} - \xi')^4}\right). \tag{10}$$

At first, we drop the cubic term. The linearized integral equation can be transformed into a "zero-energy Schrödinger equation" for $\varphi_\epsilon(\xi) \equiv \xi^{3/4}\gamma_\epsilon(\xi)$ [26]

$$[-\partial_\xi^2 + V(\xi)]\varphi_\epsilon(\xi) = 0; \quad V(\xi) = -\left(\frac{3}{16\xi^2} + \frac{\lambda}{2\xi(\tilde{\epsilon} - \xi)^2}\right). \tag{11}$$

The threshold is defined as the smallest value of $\tilde{\epsilon}$ at which the zero-energy Schrödinger equation has a nontrivial solution, which is guaranteed to be the case if the Hamiltonian $H_\varphi = -\partial_\xi^2 + V(\xi)$ is supersymmetric (SUSY) [41]. This means that H_φ can be written as $H_\varphi = Q^\dagger Q$, where $Q = \partial_\xi + W(\xi)$, $Q^\dagger = -\partial_\xi + W(\xi)$, and $W(\xi)$ is a superpotential satisfying the Riccati equation $W^2(\xi) - W'(\xi) = V(\xi)$. It can be verified [26] that the Riccati equation is solved by $W(\xi) = -3/4\xi + 1/2(\xi - \tilde{\epsilon})$ if $\tilde{\epsilon}/\lambda = -2/3$, which is the condition for H_φ to be of the SUSY type. This implies that the threshold in the self-energy is located at $\tilde{\epsilon} = -2\lambda/3 \equiv -\epsilon_0$, while the first-order equation $Q\varphi_\epsilon = 0$ yields $\gamma_\epsilon(\xi) = \xi^{-3/4}\varphi_\epsilon(\xi) = C(\tilde{\epsilon})/\sqrt{\xi + \epsilon_0}$. The function $C(\tilde{\epsilon})$ is found by substituting the last equation in Eq. (10) and retaining the cubic term. The final result for $\mathrm{Im}\Sigma$ near the threshold reads

$$\mathrm{Im}\Sigma(\xi, \epsilon) = -\sqrt{(\epsilon_0 + \tilde{\epsilon})\epsilon_0}S(\xi/\epsilon_0), \tag{12}$$

where

$$S(x) = \left(\frac{42(x+1)(2x+3)}{16x^3 + 56x^2 + 70x + 35}\right)^{1/2}. \tag{13}$$

Note that what is relevant for the observables is the threshold in $\tilde{\epsilon}$ rather than in ϵ itself. Nevertheless, we need to determine μ, as it is not guaranteed that at strong coupling electrons are still in the nondegenerate regime. Imposing the constraint of fixed number density, we find $\mu = -\epsilon_0 - (3T/2)\ln(T/E_F)$ [26]. Because $\mu < 0$ and $|\mu| \gg T$, we are indeed in the nondegenerate regime.

To find the resistivity in the nonquasiparticle regime, we ignore the vertex corrections of both ladder and Cooperon types for reasons given above. Then,

$$\rho = \frac{3m^*T}{2e^2n} \frac{\int_{-\infty}^{\infty} d\tilde{\epsilon} e^{-\tilde{\epsilon}/T} \int_0^{\infty} d\xi N(\xi)(-)\mathrm{Im}G(\xi,\epsilon)}{\int_{-\infty}^{\infty} d\tilde{\epsilon} e^{-\tilde{\epsilon}/T} \int_0^{\infty} d\xi N(\xi)\xi[\mathrm{Im}G(\xi,\epsilon)]^2}, \quad (14)$$

where $N(\xi) = m^{*3/2}\sqrt{2\xi}/\pi^2$ is the density of states. The numerator in Eq. (14) comes from the relation between the chemical potential and number density. The lower limit in the $\tilde{\epsilon}$ integrals is $-\epsilon_0$, and the Boltzmann factor $e^{-\tilde{\epsilon}/T}$ is exponentially large near $-\epsilon_0$. Therefore, the $\tilde{\epsilon}$ integrals come from the near-threshold region, where the self-energy is given by Eqs. (12) and (13). Substituting these forms into Eq. (14), we obtain

$$\rho = 5.6 \frac{m^*}{ne^2}\sqrt{T\epsilon_0} \propto T^{3/2}. \quad (15)$$

Despite the Drude-like appearance of Eq. (15), its physical content is very different because transport in this regime is controlled by off-shell electrons with $\tilde{\epsilon} \approx -\epsilon_0$ and $\xi \sim \epsilon_0$. However, if one still chooses to interpret Eq. (15) in a Drude-like way, the corresponding scattering time $\tau_D \sim E_0^{1/2}/T^{3/2}$ is shorter than the Planckian bound, $\tau_P = 1/T$, for $T \gg E_0$. In Supplemental Material [26], we show that the analytic results in Eqs. (8), (12), and (15) are confirmed by a numerical solution of Eq. (9). In particular, the inset in Fig. 2 shows the resistivity obtained by substituting a numerical solution of Eq. (9) into Eq. (14).

We now discuss briefly the role of other diagrams in Fig. 1. For $E_F \ll T \ll E_0$, the higher-order umbrella diagrams [Figs. 1(b), 1(c), etc.], provide corrections of order $\sqrt{T/E_0}$, as specified in Eq. (7). For $T \gg E_0$, it is the self-energy near the threshold that matters to transport.

Near the threshold, umbrella diagrams modify scaling function S in Eq. (12) but not the square-root singularity in $\mathrm{Im}\Sigma$ as a function of ϵ [26]. Therefore, these diagrams affect only the numerical coefficient in Eq. (15) but not the $T^{3/2}$ scaling of ρ. Next, Fig. 1(e) is a vertex correction to Fig. 1(a), which is small by an effective Migdal parameter, $m^*s^2/E_0 \sim 0.03$ [26]. Finally, Fig. 1(f) describes a four-phonon process, which gives a subleading correction to the resistivity for T below the melting temperature.

We now compare the theoretical results to the data for STO, restoring the gap (ω_0) in the phonon dispersion. The T dependence of ω_0 is obtained by substituting the measured $\epsilon_0(T)$ [36] into the LST relation [above Eq. (5)]. However, due to a partial cancellation between the T dependences of ω_0 and of the rms electron momentum, the T dependence of ω_0 does not change the results significantly [24–26]. The 2TO contribution to the resistivity is described by an interpolation formula that reproduces the analytic results at low and high T [Eqs. (8) and (15), respectively], with 2TO coupling constant g_2 as a fitting parameter. In the experiment, ρ varies faster than T^2 at higher T: a power-law fit gives $\rho \propto T^{2.7-3}$ [6,42–44]. An exponent larger than 2 was conjectured to result from multi-TO-phonon scattering [44]. However, we have shown that TO scattering gives a slower than T^2 variation of ρ for $T \gg E_0$ [cf. Eq. (15)]. An alternative explanation of the faster than T^2 dependence is scattering by LO phonons [45–48]. We adopt the latter model here and include scattering by the 58 meV LO mode within the Low-Pines approach [49], treating the Fröhlich coupling
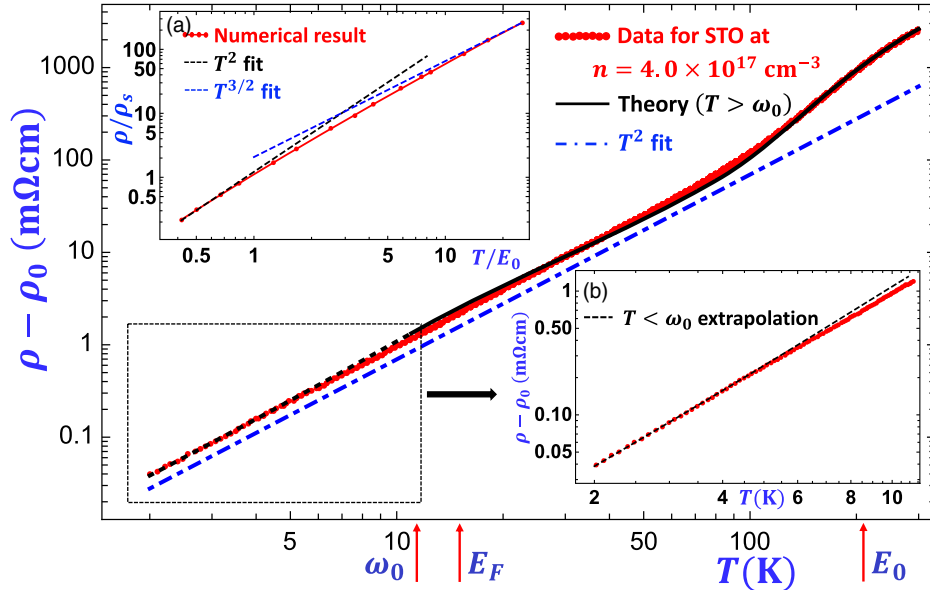

FIG. 2. Resistivity of SrTiO₃ [36] (minus the residual value ρ_0) (points, red) vs theory (solid, black), which includes scattering by two TO phonons and by the 58 meV LO phonon. An extrapolation of the theory to the regime of $T < \omega_0$ is shown by the dashed line. The dash-dotted line is a T^2 fit to the data (shifted for clarity). Insets: (a) The temperature dependence of the resistivity predicted by the 2TO model, obtained by a numerical solution of Eqs. (9) and (14), along with the fits to the asymptotic results. Here, $\rho_s = m^*E_0/ne^2$. (b) An enlargement on the low-temperature region of the main panel.

constant α as a fitting parameter; details of the fitting procedure are delegated to the Supplemental Material [26].

On the low-T side, the 2TO model should give $\rho \propto \exp(-\omega_0/T)$ for $T \ll \omega_0$, whereas the observed resistivity continues to scale down as T^2 up to the lowest T measured (2 K). Nevertheless, if we extrapolate our model to the region of $T \leq \omega_0$ (where it should not be applicable), it still provides a surprisingly good fit of the data. A fit obtained in this way is shown in Fig. 2 for $g_2 = 0.92a_0^3$ and $\alpha = 2.38$ [50]. This value of g_2, obtained from fitting over the entire range of T, is slightly larger than $0.60a_0^3$, obtained by fitting only the T^2 part of the data. To the best of our knowledge, no *ab initio* estimate of g_2 is currently available and would be highly desirable. The value of α is higher than $\alpha \approx 0.7$ [51] extracted from infrared reflectivity [52,53] and transport at high T ($200 < T < 1000$ K) [45], but consistent with other transport measurements in the intermediate temperature range ($100 < T < 200$ K) [47,54].

While we do not have a good answer to the question why the theory, extrapolated to $T < \omega_0$, still appears to describe the experiment, we note that an exponential behavior of the resistivity is obtained only if the TO mode is sharp. If it is damped (which inelastic neutron [37,55], terahertz [56], and microwave [57] spectroscopies indicate), the exponential behavior is replaced by a power-law one; however, the exponent is still larger than 2 [58]. Also, recent diagrammatic Monte Carlo calculations [59] have shown that the onset of exponential behavior for a Fröhlich polaron is shifted down to lower temperatures due to mass renormalization; a similar effect can be expected for 2TO polarons.

Finally, we note that the 2TO model provides a falsifiable prediction because the scattering mechanism in this model is (quasi)elastic. This can be verified by checking if the electron part of the thermal conductivity and the electrical conductivity obey the Wiedemann-Franz law (if the model is valid, they should) and if the optical conductivity scales with T/ω (it should not).

[1] K. A. Müller and H. Burkard, Phys. Rev. B **19**, 3593 (1979).

[2] P. Chandra, G. G. Lonzarich, S. E. Rowley, and J. F. Scott, Rep. Prog. Phys. **80**, 112502 (2017).

[3] S. Stemmer and S. J. Allen, Rep. Prog. Phys. **81**, 062502 (2018).

[4] C. Collignon, X. Lin, C. W. Rischau, B. Fauqué, and K. Behnia, Annu. Rev. Condens. Matter Phys. **10**, 25 (2019).

[5] A. Spinelli, M. A. Torija, C. Liu, C. Jan, and C. Leighton, Phys. Rev. B **81**, 155110 (2010).

[6] X. Lin, C. W. Rischau, L. Buchauer, A. Jaoui, B. Fauqué, and K. Behnia, npj Quantum Mater. **2**, 41 (2017).

[7] X. Lin, B. Fauqué, and K. Behnia, Science **349**, 945 (2015).

[8] E. Mikheev, S. Raghavan, J. Y. Zhang, P. B. Marshall, A. P. Kajdos, L. Balents, and S. Stemmer, Sci. Rep. **6**, 20865 (2016).

[9] E. McCalla, M. N. Gastiasoro, G. Cassuto, R. M. Fernandes, and C. Leighton, Phys. Rev. Mater. **3**, 022001(R) (2019).

[10] A. Sakai, T. Kanno, S. Yotsuhashi, H. Adachi, and Y. Tokura, Jpn. J. Appl. Phys. **48**, 097002 (2009).

[11] J. Engelmayer, X. Lin, C. P. Grams, R. German, T. Fröhlich, J. Hemberger, K. Behnia, and T. Lorenz, Phys. Rev. Mater. **3**, 051401(R) (2019).

[12] D. L. Maslov and A. V. Chubukov, Rep. Prog. Phys. **80**, 026503 (2017).

[13] M. W. Swift and C. G. Van de Walle, Eur. Phys. J. B **90**, 151 (2017).

[14] H. Vogt, Phys. Rev. B **51**, 8046 (1995).

[15] B. Hehlen, L. Arzel, A. Tagantsev, E. Courtens, Y. Inaba, A. Yamanaka, and K. Inoue, Physica (Amsterdam) **263-264B**, 627 (1999).

[16] A. Yamanaka, M. Kataoka, Y. Inaba, K. Inoue, B. Hehlen, and E. Courtens, Europhys. Lett. **50**, 688 (2000).

[17] P. Wölfle and A. V. Balatsky, Phys. Rev. B **98**, 104505 (2018).

[18] J. Ruhman and P. A. Lee, Phys. Rev. B **100**, 226501 (2019).

[19] J. Ruhman and P. A. Lee, Phys. Rev. B **94**, 224515 (2016).

[20] P. A. Volkov and P. Chandra, Phys. Rev. Lett. **124**, 237601 (2020).

[21] M. N. Gastiasoro, J. Ruhman, and R. M. Fernandes, Ann. Phys. (Amsterdam) **417**, 168107 (2020).

[22] M. N. Gastiasoro, T. V. Trevisan, and R. M. Fernandes, Phys. Rev. B **101**, 174501 (2020).

[23] K. L. Ngai, Phys. Rev. Lett. **32**, 215 (1974).

[24] Y. N. Epifanov, A. P. Levanyuk, and G. M. Levanyuk, Sov. Phys. Solid State Phys. **23**, 391 (1981).

[25] Y. N. Epifanov, A. P. Levanyuk, and G. M. Levanyuk, Ferroelectrics **35**, 199 (1981).

[26] See Supplemental Material at http://link.aps.org/supplemental/10.1103/PhysRevLett.126.076601 for details of the calculations, which includes Refs. [27–33].

[27] A. A. Abrikosov, L. P. Gorkov, and I. E. Dzyaloshinski, *Methods of Quantum Field Theory in Statistical Physics* (Dover, New York, 1963).

[28] A. B. Migdal, Sov. Phys. JETP **7**, 996 (1958).

[29] E. M. Lifshitz and L. P. Pitaevskii, *Physical Kinetics, Course of Theoretical Physics*, Vol. X (Butterworth-Heinemann, Burlington, 1981).

[30] S. Koshino, Prog. Theor. Phys. (Kyoto) **24**, 484 (1960).

[31] S. Koshino, Prog. Theor. Phys. (Kyoto) **24**, 1049 (1960).

[32] P. L. Taylor, Proc. Phys. Soc. **80**, 755 (1962).

[33] M. Y. Reizer and A. Sergeev, J. Exp. Theor. Phys. **65**, 1291 (1987).

[34] C. Kittel, *Quantum Theory of Solids* (Wiley & Sons, New York, 1963).

[35] The classical regime sets in for $T \gg \max\{T_{\mathrm{BG}}, \omega_0\}$, where $T_{\mathrm{BG}} = 2k_F s$ is the Bloch-Grüneisen temperature. A solution of the Boltzmann equation for 2TO scattering [26] shows that the actual crossover temperature between the classical and Bloch-Grüneisen regimes is numerically small ($0.25 T_{\mathrm{BG}}$) and below ω_0 at n considered in this Letter.

[36] K. Behnia (private communication).

[37] Y. Yamada and G. Shirane, J. Phys. Soc. Jpn. **26,** 396 (1969).

[38] X. Lin, Z. Zhu, B. Fauqué, and K. Behnia, Phys. Rev. X **3,** 021002 (2013).

[39] B. L. Altshuler, A. G. Aronov, and D. E. Khmelnitsky, J. Phys. C **15,** 7367 (1982).

[40] The mass-shell limit of the last formula reproduces the first term in Eq. (7), up to a transport correction of 2/3.

[41] F. Cooper, A. Khare, and U. Sukhatme, Phys. Rep. **251,** 267 (1995).

[42] S. H. Wemple, Phys. Rev. **137,** A1575 (1965).

[43] S. H. Wemple, A. Jayaraman, and M. DiDomenico, Phys. Rev. Lett. **17,** 142 (1966).

[44] S. H. Wemple, M. DiDomenico, and A. Jayaraman, Phys. Rev. **180,** 547 (1969).

[45] H. P. R. Frederikse and W. R. Hosler, Phys. Rev. **161,** 822 (1967).

[46] A. Baratoff and G. Binnig, Physica (Amsterdam) **108(B+C),** 1335 (1981).

[47] E. Mikheev, B. Himmetoglu, A. P. Kajdos, P. Moetakef, T. A. Cain, C. G. Van de Walle, and S. Stemmer, Appl. Phys. Lett. **106,** 062102 (2015).

[48] A. Verma, A. P. Kajdos, T. A. Cain, S. Stemmer, and D. Jena, Phys. Rev. Lett. **112,** 216601 (2014).

[49] F. E. Low and D. Pines, Phys. Rev. **98,** 414 (1955).

[50] The corresponding value of the BCS coupling constant $\lambda_{\mathrm{BCS}} = g_2^2 \Omega_0^4 m^* k_F / 8\pi^4 s^3 \approx 10^{-2}$ for $n = 10^{18}$ cm^{-3} and other parameters being the same as quoted in the text.

[51] References [52,53], $\alpha(m_e/m^*)^{1/2} = 0.5$. With $m^*/m_e = 1.8$, one obtains $\alpha = 0.7$, as mentioned in Ref. [45].

[52] D. Eagles, J. Phys. Chem. Solids **26,** 672 (1965).

[53] A. S. Barker, Phys. Rev. **145,** 391 (1966).

[54] E. Mikheev, Ph.D. Thesis, UCSB, 2016.

[55] E. Courtens, G. Coddens, B. Hennion, B. Hehlen, J. Pelous, and R. Vacher, Phys. Scr. **T49B,** 430 (1993).

[56] M. Misra, K. Kotani, I. Kawayama, H. Murakami, and M. Tonouchi, Appl. Phys. Lett. **87,** 182909 (2005).

[57] D. van der Marel (private communication).

[58] A. Kumar, V. I. Yudson, and D. L. Maslov (to be published).

[59] A. S. Mishchenko, L. Pollet, N. V. Prokof'ev, A. Kumar, D. L. Maslov, and N. Nagaosa, Phys. Rev. Lett. **123,** 076601 (2019).